HEALTH AND MEDICINE

ECM-mimetic immunomodulatory hydrogel for methicillin-resistant *Staphylococcus aureus*–infected chronic skin wound healing

Wenshuai Liu[1,2], Rui Gao[2], Chunfang Yang[2], Zujian Feng[2], Wenbin Ou-Yang[3], Xiangbin Pan[3], Pingsheng Huang[2,4], Chuangnian Zhang[2,4], Deling Kong[5], Weiwei Wang[2,4]*

The treatment of difficult-to-heal wounds remains a substantial clinical challenge due to deteriorative tissue microenvironment including the loss of extracellular matrix (ECM), excessive inflammation, impaired angiogenesis, and bacterial infection. Inspired by the chemical components, fibrous structure, and biological function of natural ECM, antibacterial and tissue environment–responsive glycopeptide hybrid hydrogel was developed for chronic wound healing. The hydrogel can facilitate the cell proliferation and macrophage polarization to M2 phenotype, and show potent antibacterial efficacy against both Gram-negative and Gram-positive bacteria. Significantly, the glycopeptide hydrogel accelerated the reconstruction of methicillin-resistant *Staphylococcus aureus* (MRSA)–infected full-thickness diabetic and scalding skin by orchestrating a pro-regenerative response indicated by abundant M2-type macrophages, attenuated inflammation, and promoted angiogenesis. Collectively, ECM-mimetic and immunomodulatory glycopeptide hydrogel is a promising multifunctional dressing to reshape the damaged tissue environment without additional drugs, exogenous cytokines, or cells, providing an effective strategy for the repair and regeneration of chronic cutaneous wounds.

INTRODUCTION

The management of difficult-to-heal cutaneous wounds caused by injuries, including burns, bruises, tears and contusions, or diseases, such as diabetes, remains highly challenging in clinic (*1*–*4*). Clinical care of chronic wounds results in huge social and economic burden, which also substantially impairs the life quality of patients (*5*). In addition, cutaneous wounds are commonly susceptible to bacterial infection because of the loss of inherent protective function of skin, which could further prevent the wound healing (*6*–*9*). To combat the infection at wounds, antibiotics are being abusively used, increasingly inducing the antibiotic resistance of pathogenic bacteria (*10*, *11*).

The wound healing cascade typically encompasses four programmed but overlapping phases including hemostasis, inflammation, cell proliferation, and tissue remodeling (*12*, *13*). Nowadays, diverse dressings have been developed for wound care. Traditional wound dressing including gauze, cotton wool, and polymer bandages cannot provide a moist environment at the wound dressing interface and are unable to prevent bacterial infection (*13*, *14*). Moreover, the removal of dressings inevitably damages the regenerative tissue. Recently, to further drive the chronic wound healing, hydrogels that have abundant water and three-dimensional (3D) structure are widely used as a platform to construct controlled delivery systems for antibacterial drugs (*15*), antioxidant agents (*16*), cytokines (*17*, *18*), or therapeutic stem cells (*19*) that could expedite the regeneration of damaged skin. However, these approaches are often limited by sophisticated manufacture, excessive components, potential drug-associated toxicity or high cost, severely impeding the clinical application. Attractively, bioactive materials could also be rationally designed and leveraged to facilitate the tissue regeneration without the presence of drugs, cytokines, or cells (*20*–*22*) by effectively directing the biological behaviors of host cells (*23*–*27*), such as cell migration, infiltration, and differentiation, and promoting the secretion of growth factors. These biomaterials or scaffolds commonly provide an optimal structural and functional microenvironment for tissue reconstruction, representing an alternative strategy in regenerative medicine. For chronic skin wound healing, it is key to exquisitely engineer a versatile dressing that could potently modulate the biological activities in the wound microenvironment including host cell behavior, inflammation, and vascularization and eliminate the bacterial infection to meet the complex and ordered process in the skin regeneration.

In recent years, biomimicry provides an innovative approach for developing multifunctional materials and devices (*22*, *27*–*29*) by replicating either the chemical components, architecture, or mechanical properties of the native tissues or organs (*30*, *31*). Most extracellular matrices (ECMs) in tissue are highly complex, dynamic, and hydrogel-like networks of hierarchically filamentous substances including polysaccharides and proteins (*32*–*34*). The ECM affords structural and mechanical support and biochemical signals for tissue development by controlling cell growth and phenotype. ECM in the diseased or injured tissue was commonly lost, thus lacking matrix for supporting constructive communication between endogenous cells and preventing the tissue repair. Here, to recapitulate the glycoprotein and collagen molecules and fibrillar architecture in ECM and the biological function of natural ECM, hybrid hydrogels assembled by dual synthetic glycopeptides were engineered to serve as an ECM-mimicking dressing for bacteria-infected cutaneous wound healing without additional therapeutic agents or cells. As shown in Fig. 1,

[1]Plastic Surgery Hospital, Chinese Academy of Medical Sciences and Peking Union Medical College, Beijing 100144, China. [2]Tianjin Key Laboratory of Biomaterial Research, Institute of Biomedical Engineering, Chinese Academy of Medical Sciences and Peking Union Medical College, Tianjin 300192, China. [3]Structural Heart Disease Center, National Center for Cardiovascular Disease, China and Fuwai Hospital, Chinese Academy of Medical Sciences and Peking Union Medical College, Beijing 100037, China. [4]Key Laboratory of Innovative Cardiovascular Devices, Chinese Academy of Medical Sciences, Beijing 100037, China. [5]College of Life Sciences, Nankai University, Tianjin 300071, China.
*Corresponding author. Email: wwwangtj@163.com, wangww@bme.pumc.edu.cn

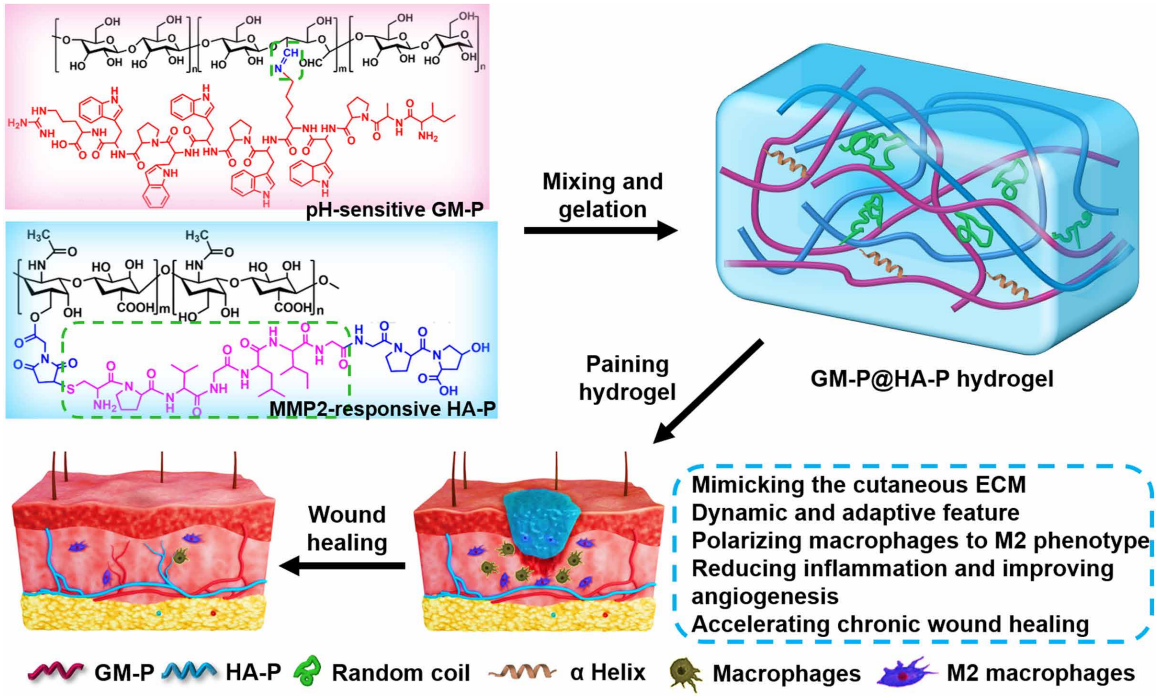

Fig. 1. Schematic diagram for the formation and application of biomimetic GM-P@HA-P glycopeptide hydrogel as a multifunctional dressing for MRSA-infected chronic skin wound healing.

glucomannan (GM) was conjugated with endogenous antibiotic peptides (ILPWKWPWWPWRR) through dynamic and acid-sensitive imine bonds (denoted as GM-P), which could mediate the macrophage polarization towards M2 type that could control the inflammation at wound site. Hyaluronic acid (HA) grafted with collagen tripeptide (GPHyp) through matrix metalloproteinase-2/9 (MMP-2/9)–responsive peptide (PVGLIG) was prepared as another glycopeptide (HA-P) that could mimic the structure support for cell adhesion, migration, and proliferation of native ECM and supply necessary amino acids for collagen reconstruction during ECM assembly. Two glycopeptides were physically mixed in water to form GM-P@HA-P hybrid hydrogel as an artificial ECM with porous structure cross-linked by hierarchical fibers with diameters ranging from nanometers to micrometers. Moreover, the dynamic pH- and MMP-2/9–responsive bonds present in glycopeptides would confer the hydrogel dynamic change and wound microenvironment–adaptive feature, which would facilitate the cell proliferation and tissue growth. In addition, the hydrogel would provide a moist environment at wounds and avoid surgical removal since it was fully degradable. Our results demonstrated that ECM-mimicking GM-P@HA-P hydrogel could prominently remodel the injured tissue environment by eradicating bacteria infection, reducing inflammation via macrophage M2 polarization, and promoting angiogenesis, which significantly expedited the skin regeneration against both methicillin-resistant *Staphylococcus aureus* (MRSA)–infected full-thickness scald wound and diabetic ulcer. Together, it is foreseeable that bioinspired GM-P@HA-P hydrogel acting as a highly effective and nontoxic dressing that could eradicate microbe and simultaneously restore chronic skin wounds holds great promise for clinical translation.

RESULTS AND DISCUSSION

Preparation and characterization of glycopeptide GM-P and HA-P

The ECM of skin tissue is a highly fibrous and porous 3D network and mainly composed of glycoprotein, collagen, and laminin, which could support cell growth and guide tissue regeneration (*35*). The decellularized skin ECM comprises hierarchical fibers with nanometer- and micrometer-scale dimensions (*36*). In addition, cutaneous ECM has good affinity with various cells that could mediate the process of wound healing. GM is a kind of polysaccharide composed of repeating mannose and glucose units, which is highly affinitive to specific cell receptors such as mannose receptors (MRs) in macrophages (*37*). HA is a linear polysaccharide that consists of alternating units of a repeating disaccharide, which is an essential component in ECM. Moreover, HA is highly involved in cellular signaling, wound repair, and matrix organization (*38*). Here, to mimic the chemical composition, spatial structure, and biological function of natural cutaneous ECM, two types of glycopeptide were prepared (Fig. 2, A and B). GM was oxidized by sodium periodate to generate multiple aldehyde and hemiacetal species in the backbone, which could react with amine to form imine linkages. The oxidized product was termed as GM-CHO, and the oxidization degree determined by colorimetric hydroxylamine titration (fig. S1) was about 23%. In addition, the molecular weight of GM-CHO was similar to that of GM, as confirmed by gel permeation chromatography analysis (fig. S2), and the characteristic stretching vibration peak for carbonyl bond in the aldehyde group was found at 1640 cm^{-1} in the Fourier transform infrared spectrum (fig. S3). All these data indicated that GM-CHO was successfully synthesized. Then, GM-peptide (GM-P) conjugate was prepared through the imine bond formation by simply

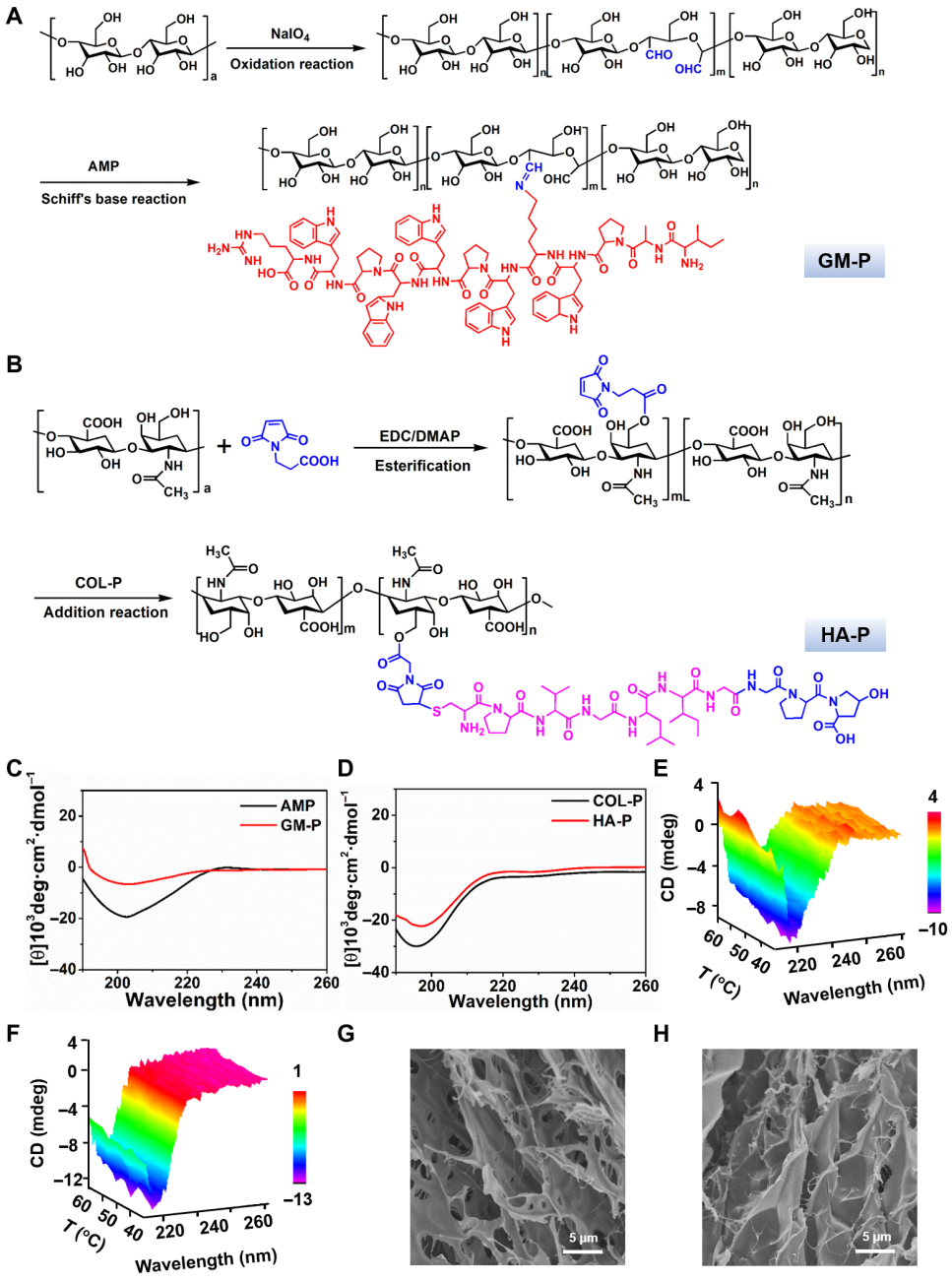

Fig. 2. Preparation and characterization of glycopeptides. (**A** and **B**) The synthesis route of GM-P (A) and HA-P (B). AMP sequence: ILPWKWPWWPWRR; COL-P sequence: GPHyp; GM-P, GM-antibacterial peptide; HA-P, hyaluronic-collagen tripeptide. (**C** and **D**) Representative CD spectrum of AMP and GM-P (C), COL-P, and HA-P and (D) in solution (0.1 mg/ml). (**E** and **F**) CD spectrum of GM-P (E) and HA-P (F) aqueous solution (0.1 mg/ml) as a function of temperature. (**G** and **H**) Representative scanning electron microscopy (SEM) images for GM-P (G) and HA-P (H) assembly in aqueous solution.

mixing GM-CHO with antimicrobial peptide (AMP) in solution. AMP is an endogenous low–molecular weight peptide with 13 amino acids (NH_2-ILPWKWPWWPWRR) and excellent antibacterial activity against both Gram-positive and Gram-negative bacteria (*39*). The chemical structure of GM-P was determined by ^{1}H NMR (proton nuclear magnetic resonance) (fig. S4), and the molar percentage of peptide graft was 8.6%.

To prepare HA-peptide (HA-P) conjugate, HA was first modified by 3-maleimide propionic acid through esterification with 1-ethyl-3-(3-dimethylaminopropyl)carbodiimide and DMAP (4-dimethylaminopyridine), and then, MMP-sensitive peptide sequence–coupled collagen tripeptide (PVGLIG-GPHyp) was grafted to HA by Michael addition at room temperature. HA-P was characterized by ^{1}H NMR (fig. S5), and the molar percentage of peptide graft was 18.5%. Collagen peptide (COL-P) is the product of enzymatic hydrolysis of collagen, which could promote cell proliferation, migration, and thus may accelerate the wound healing (*40*).

Then, the peptide conformation in HA-P and GM-P polymers was investigated by circular dichroism (CD) analysis. Figure 2C shows that native AMP (0.1 mg/ml) solution displayed a negative band with a minimum at 205 nm and a positive band with a maximum at 190 nm, which was attributed to the secondary structure of α helix. Figure 2D shows that native collagen peptide (0.1 mg/ml) solution displayed a negative band with a minimum at 196 nm, which was attributed to the secondary structure of random coil. A similar spectroscopy profile was observed for GM-P and HA-P, suggesting that the graft of peptide to GM or HA did not change the intrinsic secondary structure of polypeptide. Moreover, as the temperature increased, there was no significant change in the ellipticity of CD spectra and the overall profiles were maintained over 20° to 60°C (Fig. 2, E and F), indicating a good temperature stability of peptides in HA-P and GM-P. As shown in Fig. 2 (G and H), GM-P or HA-P alone could self-assemble into hydrogel (10%, w/w) with an irregular and plate-like structure.

Preparation and characterization of GM-P@HA-P hydrogel

To study the formation of hybrid GM-P@HA-P hydrogel, the aqueous solution of each glycopeptide was mixed at mass ratios of GM-P to HA-P at 2:1, 1:1, and 1:2. As exhibited in Fig. 3A, semisolid hydrogels were obtained at three mass ratios because of the physical cross-linking forces among polysaccharides mainly driven by hydrogen bonds (*41*). Representative scanning electron microscopy (SEM) images (Fig. 3B, top row) of GM-P@HA-P hydrogel with a mass ratio of 1:1 show highly porous network structures, and the average pore diameter (Fig. 3C) was in the range of 4.0 to 16.0 μm, while the hybrid hydrogels prepared with other mass ratios have a lower density of cross-linked network and smaller distribution of pore sizes (fig. S6). It was also observed that natural skin ECM shows a highly fibrillar and porous architecture (Fig. 3B, bottom row) with a wide pore size distribution in the range of 4.0 to 20.0 μm (Fig. 3D). Furthermore, the dimension of fibers within the hydrogel was varied from nanoscale to several micrometers. Transmission electron microscopy (fig. S7) further confirmed that GM-P@HA-P hydrogel showed ramiform nanofibrils with the diameter in the range of 20 to 30 nm. In addition, compared with the assembly of an individual glycopeptide (Fig. 2, G and H), the interpenetrating porous architecture formed by the co-assembly of dual glycopeptides was more similar with that of natural ECM. On the basis of these structural features and from the point view of biomimicry, hydrogel fabricated at a mass ratio of 1:1 was more closed to natural ECM.

Then, the mechanical properties of the composite hydrogel were examined by dynamic rheology analysis under various mechanical measurement conditions. As shown in Fig. 3E, the values of G' (storage modulus) were always greater than G'' (loss modulus) for GM-P@HA-P hydrogel within the time sweep of 0 to 1000 s, suggesting a gel state, irrespective of the different mass ratios between GM-P and HA-P. GM-P@HA-P (1:1) was used as a representative sample for the following proof-of-concept studies. Within the angular frequency of 0.1 to 100 rad/s (Fig. 3F) and the temperature range (Fig. 3G) of 10° to 50°C, GM-P@HA-P hydrogel maintained its gel state, indicating that the hydrogel was stable and temperature insensitive. As shown in Fig. 3H, the value of both G' and G'' decreased with the increasing of shear strain, suggesting the injectability or extrudability of hydrogel. When the strain reached to ~30%, G'' was over G', indicating the gel-to-sol phase transition and the destruction of the cross-linked structure of hydrogel. The self-healing property of hybrid hydrogel was then examined. Figure 3I shows that both G' and G'' modulus decreased to lower values upon applying a large strain of 50%, and the value of G' was smaller than that of G'', demonstrating a sol phase. When the strain was recovered to 5%, the sol returned to gel, indicating that GM-P@HA-P hydrogel was self-healing. Next, the self-healing properties of GM-P@HA-P hydrogel were qualitatively estimated. As shown in Fig. 3J, the separate parts cut from hydrogel could be self-assembled into one piece of hydrogel after contacting for 2 hours without external force, which was probably attributed to the reconstruction of abundant hydrogen bonds among polysaccharides (*42*). Under physiological conditions, the skin was often stretched and squeezed; thus, the self-healing property was necessary to keep the integrality of hydrogel. In addition, GM-P@HA-P hydrogel could be easily injected through a syringe equipped with a 20-gauge needle (Fig. 3K). GM-P@HA-P hydrogel was convenient for practical application. Then, the hydrogel modulus was tested as a function of time with the presence of MMP or acid. Under normal conditions, the skin surface is weakly acidic with pH varying from 4 to 6, and overexpression of MMP-2/9 and alkaline environment (pH value ≈ 7.5 to 8.9) are commonly observed in chronic or infected wound (*43*, *44*). When the bacteria were eliminated, pH values in the wound turn into neutral and then to acidic along with wound healing, which would accelerate the dissolution of GM-P@HA-P hydrogel. It was found that the modulus of GM-P@HA-P hydrogel was gradually decreased in the presence of MMP or acid pH (fig. S8), while the hydrogel was stable in alkaline pH (phosphate-buffered saline, pH ≈ 8), suggesting that the glycopeptide hydrogel was MMP and acid sensitive. Wound-environment responsivity would impart the hydrogel dynamic and tissue-adaptive properties that would enable the infiltration of host cells, benefiting the cell proliferation and tissue regeneration (*45*).

In vitro antibacterial activity of GM-P@HA-P hydrogel

Infection by drug-resistant bacteria is a great challenge for impaired skin regeneration. Next, the antimicrobial capacity of GM-P@HA-P hydrogel was investigated against Gram-positive (MRSA) and Gram-negative (*Escherichia coli*) bacteria strain. Bacteria suspensions (~10^7 colony-forming units/ml) were cocultured with GM-P@HA-P hydrogel for 24 hours. Figure 4A showed that no obvious colonies were observed in the GM-P@HA-P hydrogel group, while there was colony formation with chitosan (CS) hydrogel treatment or without treatment. The bacterial killing ratio of CS hydrogel and GM-P@HA-P was about 64.51 ± 7.67% and 96.86 ± 3.49% against MRSA and 73.65 ± 9.24% and 97.63 ± 2.85% against *E. coli*, respectively. The minimum inhibitory concentration of glycopeptide hydrogel was about 0.5 and 2 mg/ml (fig. S9) against MRSA and *E. coli*, respectively. Hence, GM-P@HA-P hydrogel had good antimicrobial efficacy toward both MRSA and *E. coli*. Then, the antibacterial mechanism was studied. The permeability of bacteria membrane was further examined by propidium iodide (PI) staining, and Hoechst 33342 was used to label bacteria. PI can penetrate the destroyed cell membrane and emit red fluorescence under excitation. Figure 4B shows strong intracellular red fluorescence signals in GM-P@HA-P hydrogel–treated bacteria after incubation for 1 hour, suggesting the disruption of cell membrane of MRSA. Afterward, the release of potassium ion (K^+) and β-galactosidase from dead MRSA was measured. As shown in Fig. 4 (C and D), GM-P@HA-P hydrogel significantly induced the leakage of both K^+ and β-galactosidase along with a time-dependent feature. These results certified that GM-P@HA-P

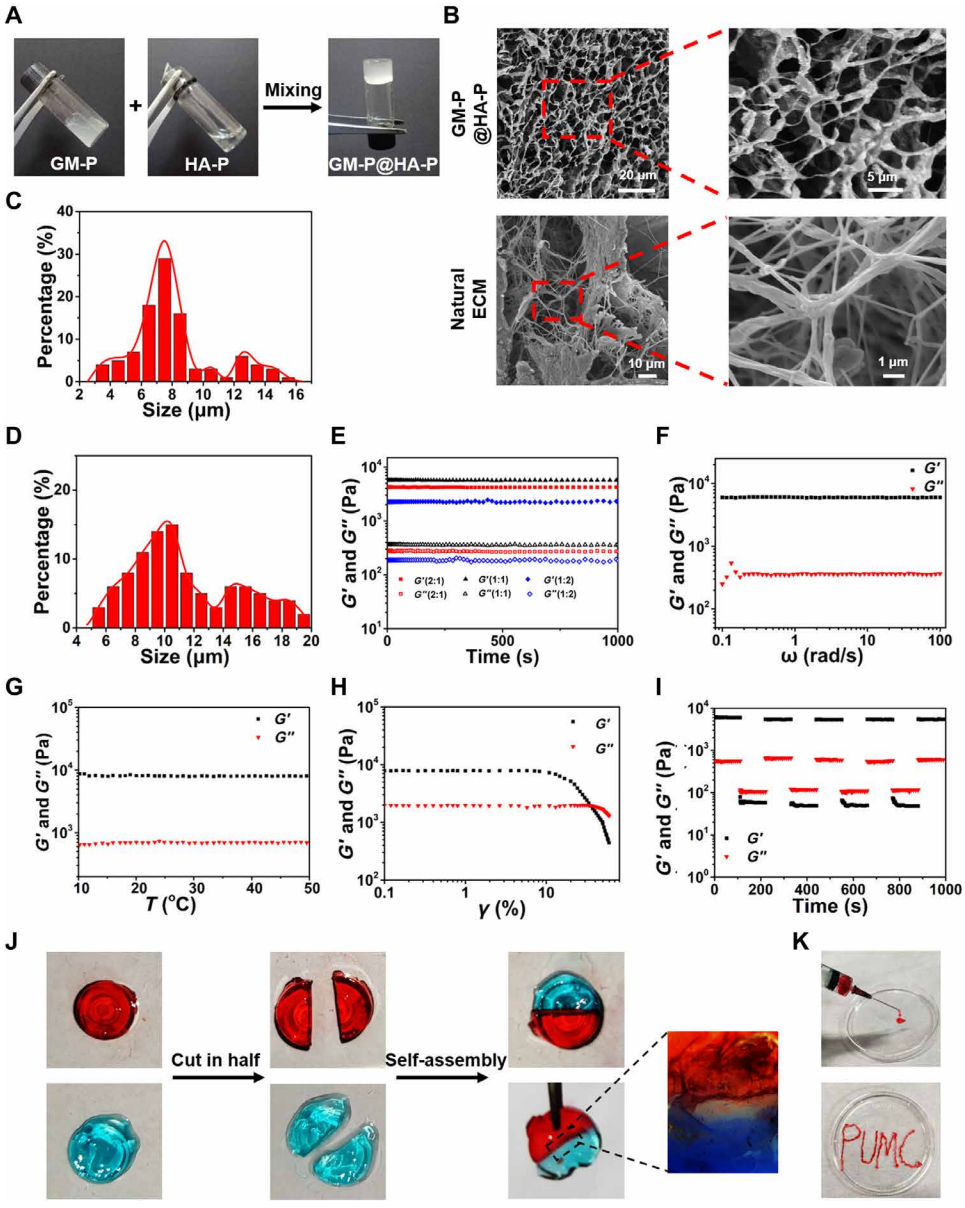

Fig. 3. Structure, mechanical, and self-healing properties of the GM-P@HA-P hydrogel. (**A**) Representative optical pictures for preparing the GM-P@HA-P hydrogel. (**B**) Representative SEM images of lyophilized GM-P@HA-P hydrogel and natural cutaneous ECM prepared by spray drying. (**C** and **D**) Diameter distribution diagram of pores in the GM-P@HA-P hydrogel (C) and natural skin ECM (D). Data represent means ± SDs ($n = 3$). (**E** to **H**) Rheological analysis of GM-P@HA-P hydrogel as a function of time (E), angular frequency (F), temperature (G), and shear strain (H). (**I**) The self-healing property of GM-P@HA-P hydrogel. (**J**) Macroscopic self-healing test of GM-P@HA-P hydrogel. Dyes for hydrogel staining were rhodamine and aniline blue for red and blue color, respectively. (**K**) Optical images of GM-P@HA-P hydrogel demonstrating the injectability.

hydrogel could break the transmembrane potential and resulted in the leakage of biomacromolecules and ion electrolytes in cytoplasm, which is in accordance with the antibacterial effect of cationic peptide polysaccharides (*46*).

A bacterial biofilm was often formed with the development of infection in wound (*47*–*49*). Therefore, the eradication of bacteria biofilm by GM-P@HA-P hydrogel was also assessed by plate culture assay. After incubating the MRSA biofilm with GM-P@HA-P hydrogel for 2 hours, intensive and strong red fluorescence signals (Fig. 4E) attributed to dead MRSA were observed. Whereas in CS hydrogel–treated biofilm, no obviously red fluorescence signal was detected. As shown in Fig. 4F, the morphology of bacteria in the biofilm treated with GM-P@HA-P hydrogel was damaged and distorted, while these in control or CS group show characteristic spherical morphology of MRSA. These data suggested that GM-P@HA-P hydrogel could destruct the established MRSA biofilm due to its superior antibacterial ability.

Cell viability, migration, tube formation, and macrophage polarization of GM-P@HA-P hydrogel

Given that the structure and biological function of GM-P@HA-P was ECM mimetic, the biological activity of hydrogel was first tested in

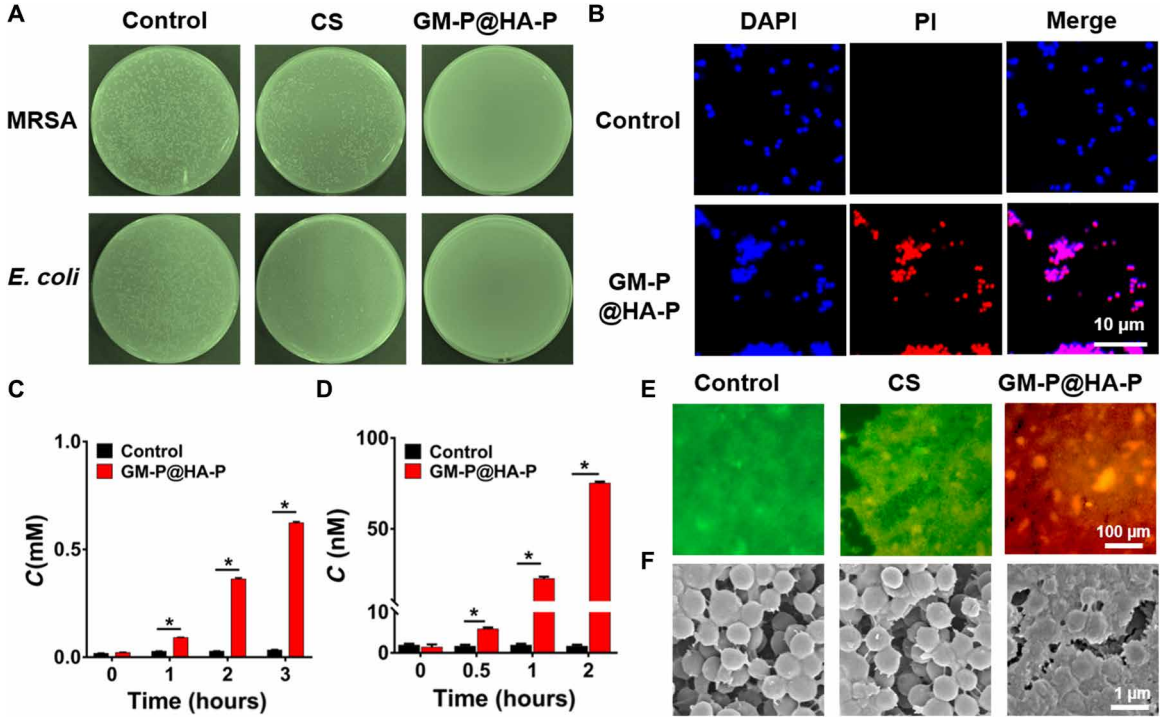

Fig. 4. In vitro antibacterial activity of GM-P@HA-P hydrogel. (**A**) Representative optical images of colony-forming units for MRSA and *E. coli* suspensions. (**B**) Fluorescence micrographs for the membrane permeability of MRSA cultured with hydrogel. Hoechst 33342 staining, blue channel; PI staining, red channel. (**C** and **D**) The concentration of K^+ (C) and β-galactosidase (D) in the culture medium of MRSA treated with GM-P@HA-P hydrogel. (**E** and **F**) Representative fluorescence and SEM images of live/dead staining assay of the MRSA biofilm treated with hydrogel. Data are shown as means ± SDs, $n = 3$. $^*P < 0.05$.

cellular level. The cytotoxicity was first tested by coculturing NIH/3T3 cells with GM-P@HA-P hydrogel. As shown in Fig. 5A, cells were widely distributed on the hydrogel and were viable, indicated by the abundance of green fluorescence dots throughout the fluorescence images obtained by live/dead assay. The cell viability (Fig. 5B) quantitatively determined by cholecystokinin-8 (CCK-8) assay demonstrated that the hydrogel showed comparable cell viability with the control group after culturing cells for 1, 4, or 7 days. These data demonstrated that GM-P@HA-P hydrogel was nontoxic to NIH/3T3 cells. In addition, the hemolysis ratio (Fig. 5C) of GM-P@HA-P hydrogel was 1.94 ± 0.28%.

Afterward, the migration of NIH/3T3 cells cultured over GM-P@HA-P hydrogel was assessed. As shown in Fig. 5 (D and E), the GM-P@HA-P hydrogel significantly enhanced the migration of NIH/3T3 cells in comparison with cells seeded in the plate. To evaluate the effect of GM-P@HA-P hydrogel on angiogenesis in vitro, the vessel-forming ability of human umbilical cord endothelial cells (HUVECs) was tested by the tube formation assay. Figure 5 (F and G) indicated that GM-P@HA-P hydrogel showed comparable ability in improving the tubule formation of HUVECs in comparison with the commercial Matrigel. These results indicated that GM-P@HA-P hydrogel not only had good cytocompatibility but also facilitated the cell proliferation, migration, and tubule formation in vitro, which may benefit the reparation and angiogenesis of impaired tissues.

Macrophages can be typically polarized into pro-inflammatory M1 or reparative M2 phenotype, which may be influenced by the biochemical properties of biomaterials (*50*, *51*). A notable feature of macrophages during M2 polarization is their elevated expression of MR, which was also known as CD206 (*24*). GM, as an MR ligand with high affinity to macrophages, may trigger intracellular signaling transduction pathways related to M2 polarization. The polarization effect of GM-P@HA-P hydrogel was examined using RAW264.7 cells, and interleukin-4 (IL-4) was used as a positive control. First, to study the changes of cell morphology after treatment, fluorescein isothiocyanate–modified phalloidin was used to label the F-actin, and the characteristic surface biomarker CD206 was used to identify M2-type macrophages. As shown in Fig. 6A, after being incubated in GM-P@HA-P hydrogel for 48 hours, RAW264.7 cells exhibited obvious pseudopod-like structures. Moreover, the elongated macrophages displayed stronger intensity of red fluorescence of CD206 staining, indicating the polarization of macrophages to M2 phenotype. Flow cytometry (Fig. 6, B to D) confirmed that the percentage of M2-type (CD206-positive) macrophages was significantly increased with the treatment of GM-P@HA-P hydrogel, while the ratio of M1-type (CD86 positive) macrophages was not obviously influenced and maintained at a low level.

Then, polymerase chain reaction (PCR) and Western blot were used to identify the signal transduction pathway for macrophage polarization. We found that the expression level of transcription factor signal transducer and activator of transcription 6 (STAT6) was significantly up-regulated by GM-P@HA-P hydrogel (Fig. 6E). IL-4 also led to the increase of STAT6 expression because IL-4–mediated M2 macrophage polarization has been well established through a Janus kinase type 1 (JAK1)–STAT6 pathway (*52*). However, there was no obvious change in the expression of p-JAK1 after GM-P@HA-P hydrogel treatment (Fig. 6, F and G), indicating that MR activation was not transmitted through the JAK1-STAT6 pathway. Furthermore, GM-P@HA-P hydrogel significantly increased

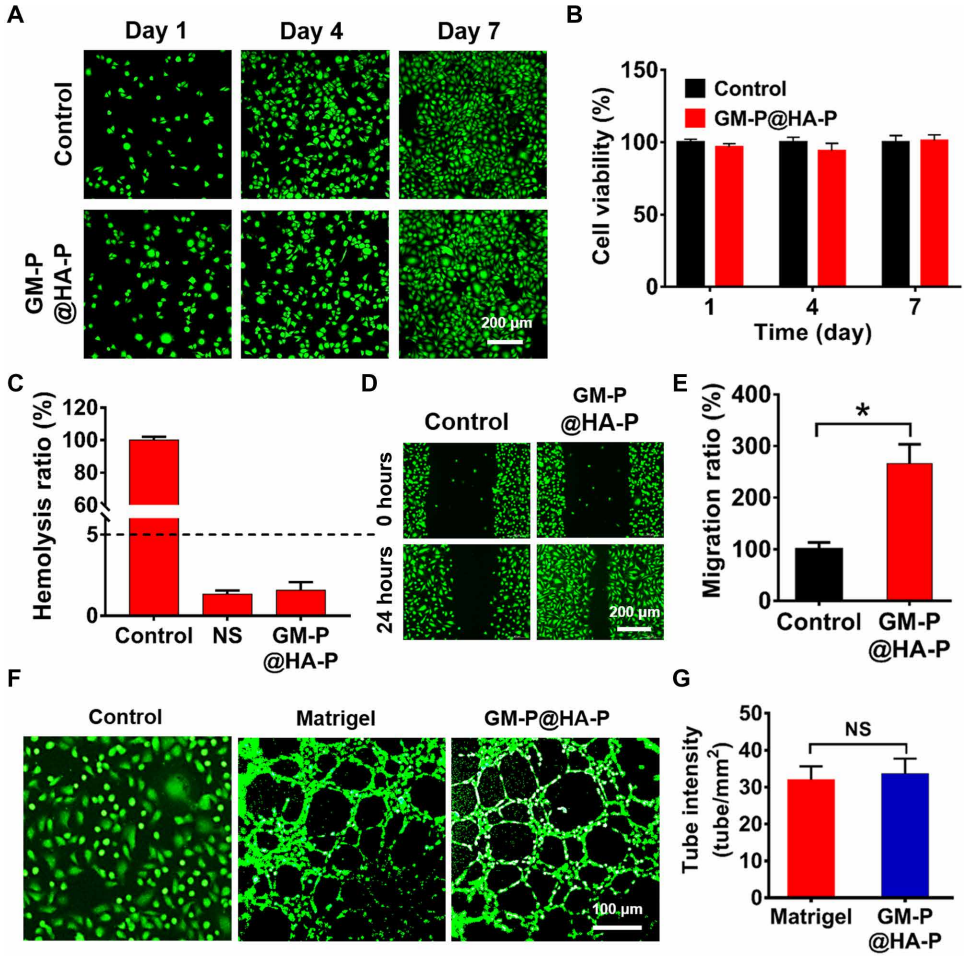

Fig. 5. In vitro cytotoxicity, migration, and tube formation of cells treated by GM-P@HA-P hydrogel. (**A**) Representative fluorescence images for NIH/3T3 cells cultured over the GM-P@HA-P hydrogel after incubation for 1, 4, and 7 days. Live cells were stained by calcein-AM (green color). Scale bar, 200 μm. (**B**) Relative viability of NIH/3T3 cells inoculated on the GM-P@HA-P hydrogel. Data are shown as means ± SDs ($n = 3$). (**C**) Hemolysis ratio of the GM-P@HA-P hydrogel. Control and NS were distilled water and normal saline solution, respectively. (**D** and **E**) The migration of NIH/3T3 cells in the culture plate or on the GM-P@HA-P hydrogel. Scale bar, 200 μm. (**F** and **G**) Tube formation of HUVECs cultured over GM-P@HA-P hydrogel. Scale bar, 100 μm. Data are shown as means ± SDs ($n = 3$). *$P < 0.05$.

the expression of extracellular signal–regulated kinase (ERK) (Fig. 6, F and G) compared with the treatment of IL-4 or untreatment. These data suggested that GM-P@HA-P hydrogel could effectively prime macrophages toward M2 phenotype through the activation of MR and following transduction by the ERK/STAT6 pathway (Fig. 6H), which may promote the treatment of chronic wound by decreasing the inflammation.

GM-P@HA-P hydrogel accelerated MRSA-infected chronic wound healing

Before therapeutic study, in vivo biocompatibility of the glycopeptide hydrogel was assessed. The degradation of hydrogel was important for in vivo treatments. If nondegradable hydrogel was resident in vivo after wound repair, then potential toxicity and other long-term safety concerns may limit its application. The degradation behavior of GM-P@HA-P hydrogel was evaluated by noninvasive fluorescence imaging. GM-P@HA-P hydrogel labeled with rhodamine was subcutaneously injected at the back of mice, and images were recorded at preconcerted time points. The fluorescence intensity (fig. S10) of GM-P@HA-P hydrogel was gradually decreased over time, demonstrating the hydrogel degradation. GM-P@HA-P hydrogel was degraded completely at 2 weeks after injection. Hematoxylin and eosin (H&E) staining of subcutaneous tissue sections from the injection sites (fig. S11) showed that no apparent histopathological structure abnormality was observed, suggesting that the GM-P@HA-P hydrogel did not cause significantly local inflammatory response. Histological assessment of major tissues (fig. S12) including heart, liver, spleen, lung, and kidney showed that the degradation of GM-P@HA-P hydrogel did not cause any damage to these organs. Blood routine parameters (fig. S13) were also in normal ranges. These data proved that GM-P@HA-P hydrogel did not induce significantly local or systemic toxicity in mice.

Then, GM-P@HA-P hydrogel was evaluated as a dressing for MRSA-infected diabetic wound. Animal models with diabetes induced by streptozotocin were constructed and used to investigate diabetic wound healing (*53*). SD (Sprague Dawley) rats with the blood glucose level over 17 mM were applied to establish MRSA-infected wounds. MRSA-infected full-thickness wounds (diameter, 1 cm) were established on the back of diabetic SD rats. Then, MRSA infection was implemented. Bacterial colonies were distinctly observed on agar plates

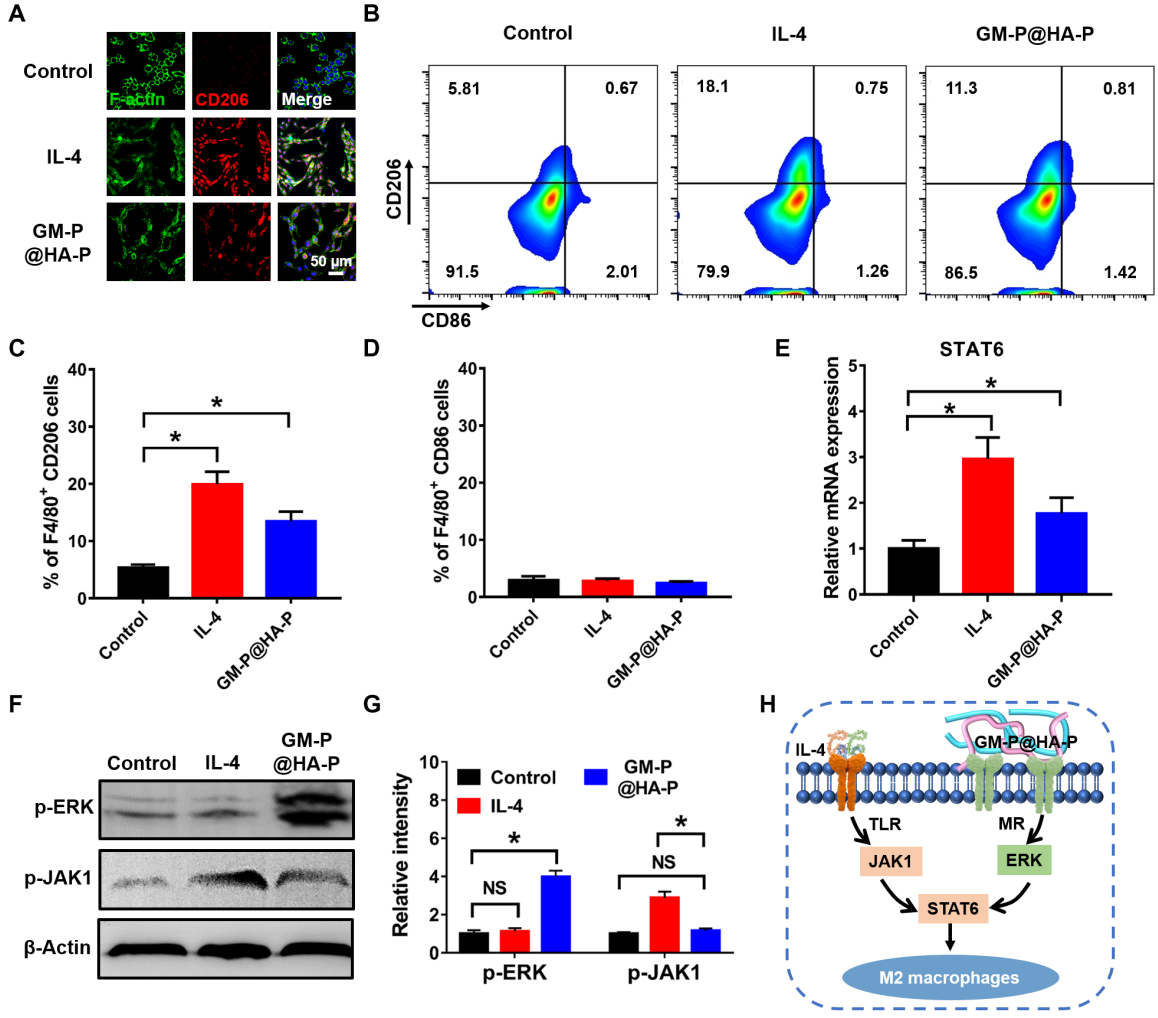

Fig. 6. Glycopeptide hydrogel effectively polarized macrophages toward M2 type. (**A**) Representative CLSM images of RAW264.7 cells treated by GM-P@HA-P hydrogel for 24 hours (red, CD206; green, F-actin; blue, cell nuclear). (**B**) Flow cytometry analysis of CD206 and CD86 expression. (**C** and **D**) The percentage of M2-type (C) ($F4/80^+CD206$) and M1-type (D) ($F4/80^+CD86$) macrophages, $n = 3$. $^*P < 0.05$. (**E**) Relative mRNA expression of STAT6. (**F** and **G**) Protein expression level of p-ERK and p-JAK1 in macrophages determined by Western blotting. $^*P < 0.05$. NS, not significant. (**H**) The mechanism of M2-type macrophage polarization induced by GM-P@HA-P hydrogel.

(fig. S14) cultured with MRSA samples collected from the infected wounds at day 1, indicating the success of MRSA infection. The hydrogel was painted onto the wound sites as a wound dressing (Fig. 7A), which could fill the tissue defect as a scaffold for in situ tissue engineering. Commercial CS hydrogel was used as positive control, owing to its antibacterial and pro-regenerative abilities in tissue repair. GM-P@HA-P hydrogel accelerated the wound healing (Fig. 7B) and significantly improved the epidermis regeneration compared with untreated or CS hydrogel–treated MRSA-infected wounds. As shown in Fig. 7C, the MRSA-infected wound without any treatment was difficult to heal, and only 55% of the wound areas were closed after 21 days partially owing to the self-contraction of murine skin wounds. However, the wound closure ratio in GM-P@HA-P hydrogel group was over 95%, which was significantly higher than that with CS hydrogel treatment (~70%). The anti-MRSA effect was further confirmed by the fact that no obvious bacterial colonies (fig. S14) were found on the plate cultured with bacteria sample from wounds treated by GM-P@HA-P hydrogel at day 21.

The histopathological structures of regenerated skin during wound healing were analyzed by H&E and Masson's trichrome staining. As shown in Fig. 7D, on the seventh day, there were many inflammatory cells but few collagen fibers in untreated wounds; however, wounds treated by GM-P@HA-P hydrogel showed abundant collagen fibers. At day 14, a few collagen fibers were observed in untreated wounds, which were still infiltrated by many inflammatory cells. Besides, a thin epithelium layer was found in the CS group. For GM-P@HA-P hydrogel–treated wounds, an epithelium layer with high regularity and dermis with abundant fibroblasts formed. At day 21, a thin epidermis was regenerated in untreated and CS-treated wounds, and more collagen fibers with random arrangement were observed. The collagen content in GM-P@HA-P hydrogel–treated wound was more than that in CS-treated wounds (fig. S15). A relatively intact epidermis and dermis with highly ordered fibrous collagen structure were observed in GM-P@HA-P hydrogel–treated wound, which were similar with the histopathological structure of normal skin tissues (fig. S16). The appearance of hair follicles also indicated the regeneration

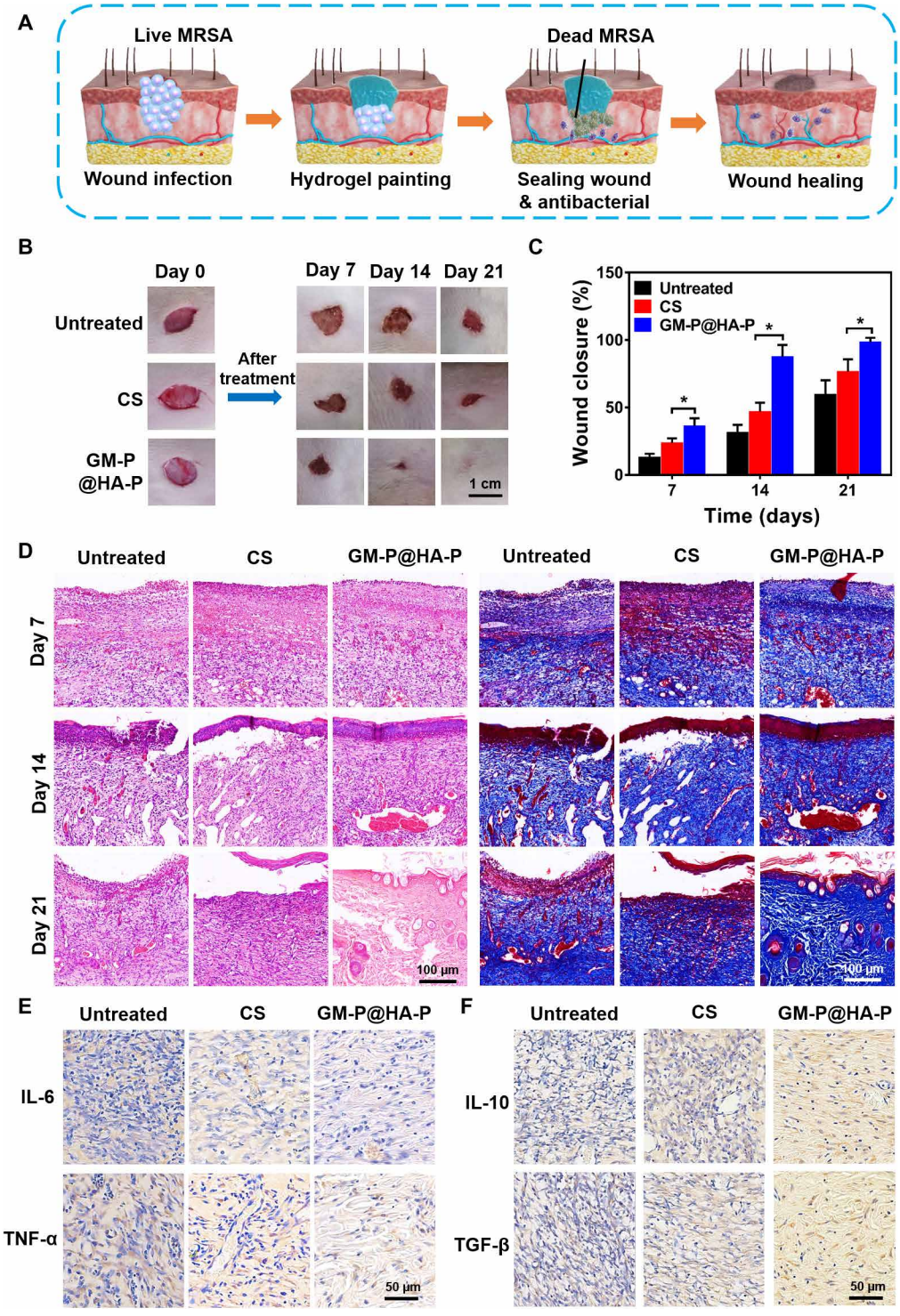

Fig. 7. GM-P@HA-P hydrogel promoted the healing of MRSA-infected full-thickness diabetic wounds in rats. (**A**) Schematic diagram of GM-P@HA-P hydrogel for wound closure and repair as a wound dressing. (**B**) Representative images of wounds during healing. (**C**) Wound closure rate at different times after wound care. Data are shown as means ± SDs ($n = 5$), *$P < 0.05$. (**D**) H&E and Masson's trichrome staining of tissue sections of skin collected from wound area at days 7, 14, and 21. (**E** and **F**) Immunohistochemical staining of IL-6 and tumor necrosis factor–α (TNF-α) (E) and IL-10 and transforming growth factor–β (TGF-β) (F) expressed in wounds at day 21.

of the dermis layer. The healed dermal tissue (Fig. 7D and fig. S17) shows that hair follicles of GM-P@HA-P group are more abundant than CS hydrogel group. Together, these results obviously demonstrated that GM-P@HA-P remarkably promoted the collagen deposition and reduced the inflammation in wound environment, by which the closure and regeneration of diabetic skin wound were accelerated.

In addition, inflammation is a major issue preventing the wound healing, which could be typically characterized by pro-inflammatory cytokines including IL-6 and tumor necrosis factor–α (TNF-α). Figure 7E and fig. S18 showed that the secretion of pro-inflammatory IL-6 and TNF-α was high in the untreated wound, demonstrating the presence of excessive inflammatory cells, which was significantly down-regulated by the treatment of hybrid glycopeptide hydrogel. The expression of anti-inflammatory IL-10 and transforming growth factor–β (TGF-β) in GM-P@HA-P group was significantly higher than these in untreated or CS hydrogel–treated wounds. Besides the pro-inflammatory cytokines, the phenotype of macrophages recruited at the injure location was also an important indicator for inflammation response. The M1-type macrophages would promote inflammation, while M2-type macrophages inhibit inflammation and promote tissue regeneration. To further illustrate the inflammation level at the wound sites, the infiltration of macrophages was investigated by immunofluorescence staining. CD86 and CD206 was chosen as a typical surface marker for M1 or M2 macrophages, respectively. As shown in Fig. 8 (A and B), compared to untreated or CS hydrogel–treated wounds, GM-P@HA-P hydrogel not only significantly decreased the percentage of CD86-positive macrophages but also increased the percentage of CD206-positive macrophages infiltrated in the wound sites at day 21, indicating a weakened inflammatory state. It was also found that the proportion of M2 macrophages was over that of M1 macrophages in the glycopeptide hydrogel–cured wounds, while CS-treated or untreated diabetic skin wounds were dominated by M1 macrophages. These data suggested that an elevated inflammation remained at the untreated diabetic skin wound and GM-P@HA-P hydrogel could effectively ameliorate the local inflammatory response and transform the tissue microenvironment from inflammatory to reparative by polarizing naive macrophages recruited at the wound to M2 type and promoting the secretion of anti-inflammatory cytokine and TGF.

Angiogenesis is required for tissue remodeling. M2 macrophages can promote the proliferation and differentiation of vascular endothelial cell by secreting vascular endothelial growth factors to stimulate angiogenesis (*54*, *55*). CD31 is a transmembrane protein expressed in early angiogenesis, demonstrating the neovascularization, while α–smooth muscle actin (α-SMA) is a cytoplasmic protein expressed in later angiogenesis, indicating the maturation of vascular smooth muscle cells. As shown in Fig. 8C, remarkable angiogenesis was found in GM-P@HA-P hydrogel–treated wounds, and the relative fluorescence intensity of anti-CD31 and α-SMA antibody (Fig. 8C) indicated a significantly higher density of vessels in dermis from wounds cured by GM-P@HA-P, compared with that in control and CS hydrogel–treated groups. Collectively, the glycopeptide hydrogel could effectively reduce the inflammation and improve the angiogenesis at the diabetic wound. It could also be concluded that controlling the macrophage polarization was efficient in alleviating the inflammation level at the wound site. Furthermore, the epidermis thickness was examined by immunofluorescent staining of the keratin expression in the wound sites. Keratin was a vital branch of fibrin, mainly expressed in epithelium (*56*). As shown in Fig. 8D, the secretion level of cytokeratin 14 (CK 14) protein in control and CS groups was significantly higher than that in the GM-P@HA-P hydrogel group at day 21. Besides, the renascent epithelial thickness stained by CK 14 in the hybrid glycopeptide hydrogel group was significantly lower in comparison with that in CS-treated wounds. Together, GM-P@HA-P hydrogel could expedite the regeneration of infected diabetic wounds by promoting the reconstruction of epidermis and mature dermis layer characterized by ordered collagen fibrils, abundant hair follicles, and thin keratin layer.

Last, the pro-healing effect of GM-P@HA-P hydrogel was tested on another representative chronic wound model, MRSA-infected scald skin wound. Results (figs. S19 to S21) demonstrated that GM-P@HA-P hydrogel could accelerate the regeneration of MRSA-infected scald wounds in SD rats, which, on its own, could effectively clear MRSA infection, reduce inflammation, facilitate angiogenesis and blood vessel maturation, and accelerate the remodeling of skin pathological structure. Furthermore, apart from hydrogels, dressings based on slippery textile or ion-loaded niacin metal-organic framework were fabricated by microfluidic electrospray or printing to cure hard-to-heal wounds (*57*, *58*) by focusing on biological processes commonly occurring during wound healing, including fluid exudation and the secretion of reactive oxygen species in damaged tissue. Such dressings could either drain tissue fluids from the wound or provide a controlled release of copper and zinc ions, resulting in superior antioxidant capability. Reduced inflammation, promoted angiogenesis, and enhanced collagen deposition were observed in infected full-thickness skin defect model. However, few approaches have been focusing on the substitution of defected tissue ECM with an inherently bioactive hydrogel. Our ECM-mimicking and immunomodulatory glycopeptide hydrogel demonstrated great advantage in normalizing the deteriorative tissue microenvironment in chronic wounds, without the use of anti-inflammatory drugs, cytokines, or mineral salts. In addition, more hybrid hydrogels could be generated by adjusting the mass ratio between glycopeptides or selecting other types of bioactive polysaccharides or peptides. These data convincingly demonstrated that the synthetic, ECM-mimicking, and immunomodulatory glycopeptide hydrogel could reshape the deteriorative environment in chronic wounds including infected diabetic and scald skin injury and facilitate a valid reparative tissue regeneration. According to these excellent properties obtained in this work, the regeneration of skin appendages including hair follicles and sweat glands and the recovery of skin functions will be included in future endeavors.

In summary, inspired by the composition, structure, and function of ECM, a type of man-made hybrid hydrogel with total glycopeptide components and 3D fibrous network structure was successfully manufactured. The hybrid glycopeptide significantly promoted the cutaneous healing and regeneration in chronic skin injuries, including diabetic and scald wounds. Compared with the present hydrogel-based systems for wound healing, the resultant GM-P@HA-P hydrogel in this work owns the following advantages: (i) ECM-mimicking design principle including total biocompatible polysaccharide and peptide components, highly fibrillar network architecture with hierarchical fiber diameters, wound-environment adaptivity, and cell modulation ability such as improving cell adhesion, migration, and proliferation; (ii) facile, mild, and low-cost hydrogel manufacturing: self-assembly in aqueous solution at room temperature without chemical cross-linking or external light irradiation, tunable composition, and good injectability with self-healing property; (iii) excellent inherent antibacterial ability against drug-resistant bacteria strains

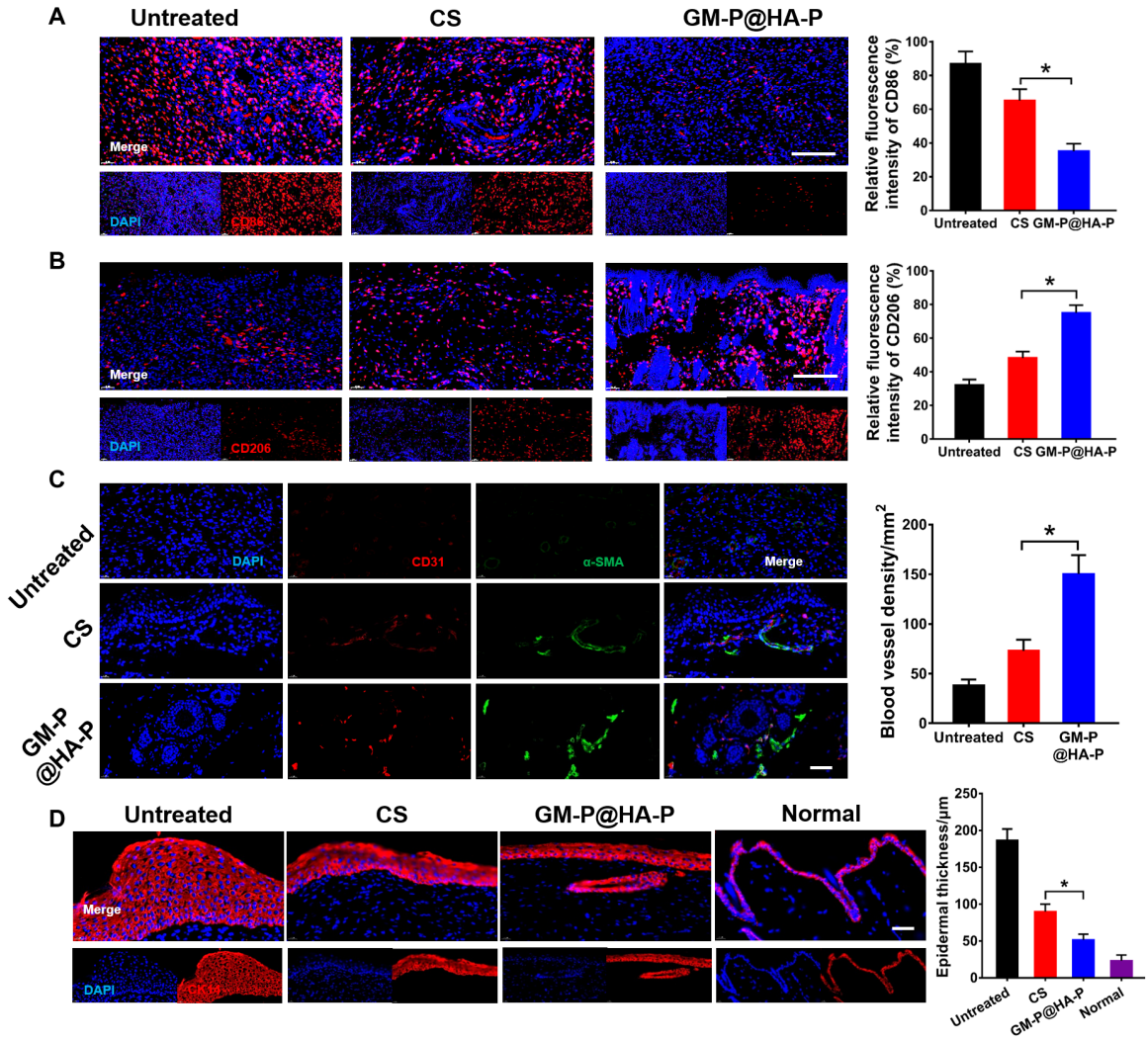

Fig. 8. GM-P@HA-P hydrogel promoted M2-type macrophage polarization and angiogenesis during the wound healing. (**A** and **B**) Representative immunofluorescence images and quantification analysis of macrophage phenotype in the regenerated skin tissues on day 21 after diabetic wound healing. Macrophages were stained with CD86 (A) or CD206 (B) in red, and the nuclei were stained with 4′,6-diamidino-2-phenylindole (DAPI) in blue. Scale bar, 100 μm. (**C**) Representative immunofluorescence images of CD31 (red)/α-SMA (green) staining in the regenerated skin tissues and quantification of blood vessel density on day 21 after wound healing. Nuclei were stained with DAPI in blue. Scale bar, 50 μm. (**D**) Representative immunofluorescence images for CK 14 staining to show the epidermal thickness. The epithelial cells were stained with CK 14 in red, and the nuclei were stained with DAPI in blue. Scale bar, 50 μm. *$P < 0.05$.

without the use of metal oxide or antibiotic; (iv) totally biodegradable and biocompatible; (v) the hydrogel could relieve the detrimental inflammation and promote angiogenesis through polarizing macrophages into M2 type as transmitted by MR-ERK-STAT6 signaling pathway; and (vi) restore the histopathological structure of chronic skin wounds in the absence of cytokines, drugs, nuclei acids, or therapeutic cells. Overall, the bioinspired GM-P@HA-P hydrogel was a promising wound dressing that could augment the repair and regeneration of cutaneous tissue, which may be extensively used in the management of chronic wounds caused by burns, cuts, diabetes, and so on.

MATERIALS AND METHODS

Materials and reagents

The AMP (ILPWKWPWWPWRR) and collagen peptides (C-PVGLIG-GPHyp) were purchased from Bankpeptide biological technology Co. Ltd (Hefei, China). GM ($\eta \geq 15\,000$ mPa·s) and HA was purchased from Sigma-Aldrich (St. Louis, USA). All animal experimental procedures were approved by Animal Experiment Ethics Committee and Authority of Institute of Radiation Medicine, Chinese Academy of Medical Sciences [approval no. SYXK (Jin) 2019-0002].

Synthesis and characterization of GM-P and HA-P

GM-P was prepared through the formation of imine bonds via Schiff's base reaction between the oxidated GM and peptide. Typically, 100 μl of AMP solution [5 weight % (wt %)] and 100 μl of GM-CHO solution (5 wt %) were mixed at room temperature, and the reaction was continued for 24 hours. GM-P was obtained by dialysis against water and lyophilization. Details for the synthesis and characterization of GM-CHO were provided in the Supplementary Materials.

HA-P was prepared by the Michael addition reaction between maleimide-decorated HA and collagen peptide. Briefly, 1 ml of collagen peptide solution (5 wt %) and 1 ml of HA-maleimide solution (5 wt %) were mixed and reacted for 24 hours at room temperature. After dialysis against deionized water for 72 hours, HA-P was obtained by lyophilization. The structure of GM-P and HA-P was characterized by ^{1}H NMR. Synthesis for maleimide-decorated HA was shown in the Supplementary Materials.

Fabrication and characterization of GM-P@HA-P hydrogel

The hybrid GM-P@HA-P hydrogel was fabricated by simply mixing the two kinds of glycopeptides in aqueous solution at various mass ratios. The gelation occurred in 1 min upon vortex. The interior morphology of glycopeptide hydrogel was investigated by SEM (Hitachi S-4800, Japan). GM-P@HA-P hydrogel was quick-frozen in liquid nitrogen and lyophilized, and at least three random areas were captured for analyzing the morphology of the hydrogels. The rheology properties of hydrogels were evaluated by an AR 2000ex rheometer (TA Instruments).

In vitro antibacterial activity and mechanism

The antimicrobial activity and mechanism of GM-P@HA-P hydrogel were determined by shaking culture method, PI staining, and the leakage of K^+ and β-galactosidase against MRSA and *E. coli*. Bacterial biofilms of MRSA were also treated with hydrogels and observed by SEM (FEI Quanta 200, Holland). Details for these experiments are described in the Supplementary Materials.

Cytocompatibility evaluation of GM-P@HA-P hydrogel

Cytotoxicity of GM-P@HA-P hydrogel was evaluated on the NIH/3T3 cells by CCK-8 and live/dead assay. The hemolysis of hydrogel was studied using fresh rabbit whole blood. The migration of NIH/3T3 cells and tube formation of HUVECs on the hydrogel were also examined. Details for these experiments were provided in the Supplementary Materials.

Macrophage activation by hydrogel

Macrophage polarization of GM-P@HA-P hydrogel was evaluated on the RAW264.7 cells by flow cytometry and observed by CLSM (confocal laser scanning microscopy). Reverse transcription PCR and Western blot were used to determine the potential cellular signal transduction pathway for macrophage polarization. Details for these experiments were provided in the Supplementary Materials.

MRSA-infected chronic wound healing in vivo

The infected-wound model of full-thickness defective skin wounds in diabetic SD rats wounds (diameter, 1 cm) or scald skin wounds (diameter, 2 cm) in normal SD rats were produced on the back. At predetermined times, the volume of wounds was photographed and measured to calculate the wound closure rate. The skin tissues of wound site were harvested to assess the wound healing process by H&E, Masson's trichrome, immunohistochemical, and immunofluorescence staining. Detailed experimental procedures were shown in the Supplementary Materials.

Statistical analysis

Data are shown as means ± SDs. Differences between two groups were analyzed by Student's *t* test. One-way analysis of variance (ANOVA) was used to assess the difference between multiple groups. $P < 0.05$ was considered statistically significant.

SUPPLEMENTARY MATERIALS

Supplementary material for this article is available at https://science.org/doi/10.1126/sciadv.abn7006

View/request a protocol for this paper from *Bio-protocol*.

REFERENCES AND NOTES

1. B. K. Sun, Z. Siprashvili, P. A. Khavari, Advances in skin grafting and treatment of cutaneous wounds. *Science* **346**, 941–945 (2014).
2. S. L. Wong, M. Demers, K. Martinod, M. Gallant, Y. Wang, A. B. Goldfine, C. R. Kahn, D. D. Wagner, Diabetes primes neutrophils to undergo NETosis, which impairs wound healing. *Nat. Med.* **21**, 815–819 (2015).
3. A. J. Singer, A. B. Dagum, Current management of acute cutaneous wounds. *N. Engl. J. Med.* **359**, 1037–1046 (2008).
4. V. Falanga, Wound healing and its impairment in the diabetic foot. *Lancet* **366**, 1736–1743 (2005).
5. J. A. Haagsma, N. Graetz, I. Bolliger, M. Naghavi, H. Higashi, E. C. Mullany, S. F. Abera, J. P. Abraham, K. Adofo, U. Alsharif, E. A. Ameh, W. Ammar, C. A. Antonio, L. H. Barrero, T. Bekele, D. Bose, A. Brazinova, F. Catala-Lopez, L. Dandona, R. Dandona, P. I. Dargan, D. De Leo, L. Degenhardt, S. Derrett, S. D. Dharmaratne, T. R. Driscoll, L. Duan, S. P. Ermakov, F. Farzadfar, V. L. Feigin, R. C. Franklin, B. Gabbe, R. A. Gosselin, N. Hafezi-Nejad, R. R. Hamadeh, M. Hijar, G. Hu, S. P. Jayaraman, G. Jiang, Y. S. Khader, E. A. Khan, S. Krishnaswami, C. Kulkarni, F. E. Lecky, R. Leung, R. Lunevicius, R. A. Lyons, M. Majdan, A. J. Mason-Jones, R. Matzopoulos, P. A. Meaney, W. Mekonnen, T. R. Miller, C. N. Mock, R. E. Norman, R. Orozco, S. Polinder, F. Pourmalek, V. Rahimi-Movaghar, A. Refaat, D. Rojas-Rueda, N. Roy, D. C. Schwebel, A. Shaheen, S. Shahraz, V. Skirbekk, K. Soreide, S. Soshnikov, D. J. Stein, B. L. Sykes, K. M. Tabb, A. M. Temesgen, E. Y. Tenkorang, A. M. Theadom, B. X. Tran, T. J. Vasankari, M. S. Vavilala, V. V. Vlassov, S. M. Woldeyohannes, P. Yip, N. Yonemoto, M. Z. Younis, C. Yu, C. J. Murray, T. Vos, The global burden of injury: Incidence, mortality, disability-adjusted life years and time trends from the global burden of disease study 2013. *Inj. Prev.* **22**, 3–18 (2016).
6. Y. Qiao, J. He, W. Chen, Y. Yu, W. Li, Z. Du, T. Xie, Y. Ye, S. Y. Hua, D. Zhong, K. Yao, M. Zhou, Light-activatable synergistic therapy of drug-resistant bacteria-infected cutaneous chronic wounds and nonhealing keratitis by cupriferous hollow nanoshells. *ACS Nano* **14**, 3299–3315 (2020).
7. W. Liu, C. Yang, R. Gao, C. Zhang, W. Ou-Yang, Z. Feng, C. Zhang, X. Pan, P. Huang, D. Kong, W. Wang, Polymer composite sponges with inherent antibacterial, hemostatic, inflammation-modulating and proregenerative performances for methicillin-resistant *Staphylococcus aureus*-infected wound healing. *Adv. Healthc. Mater.* **10**, e2101247 (2021).
8. L. Zhou, Y. Xi, Y. Xue, M. Wang, Y. Liu, Y. Guo, B. Lei, Injectable self-healing antibacterial bioactive polypeptide-based hybrid nanosystems for efficiently treating multidrug resistant infection, skin-tumor therapy, and enhancing wound healing. *Adv. Funct. Mater.* **29**, 1806883 (2019).
9. W. Liu, W. Ou-Yang, C. Zhang, Q. Wang, X. Pan, P. Huang, C. Zhang, Y. Li, D. Kong, W. Wang, Synthetic polymeric antibacterial hydrogel for methicillin-resistant *Staphylococcus aureus*-infected wound healing: Nanoantimicrobial self-assembly, drug- and cytokine-free strategy. *ACS Nano* **14**, 12905–12917 (2020).
10. X. Li, S. M. Robinson, A. Gupta, K. Saha, Z. Jiang, D. F. Moyano, A. Sahar, M. A. Riley, V. M. Rotello, Functional gold nanoparticles as potent antimicrobial agents against multi-drug-resistant bacteria. *ACS Nano* **8**, 10682–10686 (2014).
11. V. Thammavongsa, H. K. Kim, D. Missiakas, O. Schneewind, Staphylococcal manipulation of host immune responses. *Nat. Rev. Microbiol.* **13**, 529–543 (2015).
12. M. Kharaziha, A. Baidya, N. Annabi, Rational design of immunomodulatory hydrogels for chronic wound healing. *Adv. Mater.* **33**, e2100176 (2021).
13. S. O. Blacklow, J. Li, B. R. Freedman, M. Zeidi, C. Chen, D. J. Mooney, Bioinspired mechanically active adhesive dressings to accelerate wound closure. *Sci. Adv.* **5**, eaaw3963 (2019).
14. X. Zhao, H. Wu, B. Guo, R. Dong, Y. Qiu, P. X. Ma, Antibacterial anti-oxidant electroactive injectable hydrogel as self-healing wound dressing with hemostasis and adhesiveness for cutaneous wound healing. *Biomaterials* **122**, 34–47 (2017).
15. S. Li, S. Dong, W. Xu, S. Tu, L. Yan, C. Zhao, J. Ding, X. Chen, Antibacterial hydrogels. *Adv. Sci.* **5**, 1700527 (2018).
16. X. Zhao, Y. Liang, Y. Huang, J. He, Y. Han, B. Guo, Physical double-network hydrogel adhesives with rapid shape adaptability, fast self-healing, antioxidant and NIR/pH stimulus-responsiveness for multidrug-resistant bacterial infection and removable wound dressing. *Adv. Funct. Mater.* **30**, 1910748 (2020).
17. G. Chen, Y. Yu, X. Wu, G. Wang, J. Ren, Y. Zhao, Bioinspired multifunctional hybrid hydrogel promotes wound healing. *Adv. Funct. Mater.* **28**, 1801386 (2018).
18. C. Chen, Y. Liu, H. Wang, G. Chen, X. Wu, J. Ren, H. Zhang, Y. Zhao, Multifunctional chitosan inverse opal particles for wound healing. *ACS Nano* **12**, 10493–10500 (2018).
19. N. C. Cheng, W. J. Lin, T. Y. Ling, T. H. Young, Sustained release of adipose-derived stem cells by thermosensitive chitosan/gelatin hydrogel for therapeutic angiogenesis. *Acta Biomater.* **51**, 258–267 (2017).

20. M. M. Islam, M. Shahruzzaman, S. Biswas, M. Nurus Sakib, T. U. Rashid, Chitosan based bioactive materials in tissue engineering applications—A review. *Bioact. Mater.* **5**, 164–183 (2020).
21. T. L. Lopez-Silva, D. G. Leach, A. Azares, I. C. Li, D. G. Woodside, J. D. Hartgerink, Chemical functionality of multidomain peptide hydrogels governs early host immune response. *Biomaterials* **231**, 119667 (2020).
22. Z. Feng, Q. Su, C. Zhang, P. Huang, H. Song, A. Dong, D. Kong, W. Wang, Bioinspired nanofibrous glycopeptide hydrogel dressing for accelerating wound healing: A cytokine-free, M2-type macrophage polarization approach. *Adv. Funct. Mater.* **30**, 2006454 (2020).
23. Y. Li, Y. Xiao, C. Liu, The horizon of materiobiology: A perspective on material-guided cell behaviors and tissue engineering. *Chem. Rev.* **117**, 4376–4421 (2017).
24. J. Gan, Y. Dou, Y. Li, Z. Wang, L. Wang, S. Liu, Q. Li, H. Yu, C. Liu, C. Han, Z. Huang, J. Zhang, C. Wang, L. Dong, Producing anti-inflammatory macrophages by nanoparticle-triggered clustering of mannose receptors. *Biomaterials* **178**, 95–108 (2018).
25. F. Bao, G. Pei, Z. Wu, H. Zhuang, Z. Zhang, Z. Huan, C. Wu, J. Chang, Bioactive self-pumping composite wound dressings with micropore array modified janus membrane for enhanced diabetic wound healing. *Adv. Funct. Mater.* **30**, 2005422 (2020).
26. X. Zhang, D. Yao, W. Zhao, R. Zhang, B. Yu, G. Ma, Y. Li, D. Hao, F. J. Xu, Engineering platelet-rich plasma based dual-network hydrogel as a bioactive wound dressing with potential clinical translational value. *Adv. Funct. Mater.* **31**, 2009258 (2021).
27. R. R. Naik, S. Singamaneni, Introduction: Bioinspired and biomimetic materials. *Chem. Rev.* **117**, 12581–12583 (2017).
28. Y. Wang, S. E. Naleway, B. Wang, Biological and bioinspired materials: Structure leading to functional and mechanical performance. *Bioact. Mater.* **5**, 745–757 (2020).
29. E. Prince, E. Kumacheva, Design and applications of man-made biomimetic fibrillar hydrogels. *Nat. Rev. Mater.* **4**, 99–115 (2019).
30. P. Zhang, Y. Jiang, D. Liu, Y. Liu, Q. Ke, H. Xu, A bioglass sustained-release scaffold with ECM-like structure for enhanced diabetic wound healing. *Nanomedicine* **15**, 2241–2253 (2020).
31. C. E. Witherel, K. Sao, B. K. Brisson, B. Han, S. W. Volk, R. J. Petrie, L. Han, K. L. Spiller, Regulation of extracellular matrix assembly and structure by hybrid M1/M2 macrophages. *Biomaterials* **269**, 120667 (2021).
32. T. Dvir, B. P. Timko, D. S. Kohane, R. Langer, Nanotechnological strategies for engineering complex tissues. *Nat. Nanotechnol.* **6**, 13–22 (2011).
33. H. Geckil, F. Xu, X. Zhang, S. Moon, U. Demirci, Engineering hydrogels as extracellular matrix mimics. *Nanomedicine* **5**, 469–484 (2010).
34. S. Pina, J. M. Oliveira, R. L. Reis, Natural-based nanocomposites for bone tissue engineering and regenerative medicine: A review. *Adv. Mater.* **27**, 1143–1169 (2015).
35. Q. Zhang, J. A. Johnson, L. W. Dunne, Y. Chen, T. Iyyanki, Y. Wu, E. I. Chang, C. D. Branch-Brooks, G. L. Robb, C. E. Butler, Decellularized skin/adipose tissue flap matrix for engineering vascularized composite soft tissue flaps. *Acta Biomater.* **35**, 166–184 (2016).
36. B. M. Gillette, N. S. Rossen, N. Das, D. Leong, M. Wang, A. Dugar, S. K. Sia, Engineering extracellular matrix structure in 3D multiphase tissues. *Biomaterials* **32**, 8067–8076 (2011).
37. H. Chen, J. Cheng, L. Ran, K. Yu, B. Lu, G. Lan, F. Dai, F. Lu, An injectable self-healing hydrogel with adhesive and antibacterial properties effectively promotes wound healing. *Carbohydr. Polym.* **201**, 522–531 (2018).
38. J. Gan, C. Liu, H. Li, S. Wang, Z. Wang, Z. Kang, Z. Huang, J. Zhang, C. Wang, D. Lv, L. Dong, Accelerated wound healing in diabetes by reprogramming the macrophages with particle-induced clustering of the mannose receptors. *Biomaterials* **219**, 119340 (2019).
39. E. Mataraci, S. Dosler, In vitro activities of antibiotics and antimicrobial cationic peptides alone and in combination against methicillin-resistant *Staphylococcus aureus* biofilms. *Antimicrob. Agents Chemother.* **56**, 6366–6371 (2012).
40. S. Fahmy-Garcia, D. Mumcuoglu, L. de Miguel, V. Dieleman, J. Witte-Bouma, B. C. J. van der Eerden, M. van Driel, D. Eglin, J. A. N. Verhaar, S. Kluijtmans, G. van Osch, E. Farrell, Novel in situ gelling hydrogels loaded with recombinant collagen peptide microspheres as a slow-release system induce ectopic bone formation. *Adv. Healthc. Mater.* **7**, e1800507 (2018).
41. Y. Liang, J. Xue, B. Du, J. Nie, Ultrastiff, tough, and healable ionic-hydrogen bond cross-linked hydrogels and their uses as building blocks to construct complex hydrogel structures. *ACS Appl. Mater. Interfaces* **11**, 5441–5454 (2019).
42. A. Pena-Francesch, H. Jung, M. C. Demirel, M. Sitti, Biosynthetic self-healing materials for soft machines. *Nat. Mater.* **19**, 1230–1235 (2020).
43. S. A. Castleberry, B. D. Almquist, W. Li, T. Reis, J. Chow, S. Mayner, P. T. Hammond, Self-assembled wound dressings silence MMP-9 and improve diabetic wound healing in vivo. *Adv. Mater.* **28**, 1809–1817 (2016).
44. Y. Zhu, J. Zhang, J. Song, J. Yang, Z. Du, W. Zhao, H. Guo, C. Wen, Q. Li, X. Sui, L. Zhang, A multifunctional pro-healing zwitterionic hydrogel for simultaneous optical monitoring of ph and glucose in diabetic wound treatment. *Adv. Funct. Mater.* **30**, 1905493 (2019).
45. Q. Feng, K. Wei, S. Lin, Z. Xu, Y. Sun, P. Shi, G. Li, L. Bian, Mechanically resilient, injectable, and bioadhesive supramolecular gelatin hydrogels crosslinked by weak host-guest interactions assist cell infiltration and in situ tissue regeneration. *Biomaterials* **101**, 217–228 (2016).
46. P. Li, C. Zhou, S. Rayatpisheh, K. Ye, Y. F. Poon, P. T. Hammond, H. Duan, M. B. Chan-Park, Cationic peptidopolysaccharides show excellent broad-spectrum antimicrobial activities and high selectivity. *Adv. Mater.* **24**, 4130–4137 (2012).
47. X. Ding, S. Duan, X. Ding, R. Liu, F.-J. Xu, Versatile antibacterial materials: An emerging arsenal for combatting bacterial pathogens. *Adv. Funct. Mater.* **28**, 1802140 (2018).
48. D. Hu, Y. Deng, F. Jia, Q. Jin, J. Ji, Surface charge switchable supramolecular nanocarriers for nitric oxide synergistic photodynamic eradication of biofilms. *ACS Nano* **14**, 347–359 (2020).
49. Y. Zhu, C. Xu, N. Zhang, X. Ding, B. Yu, F.-J. Xu, Polycationic synergistic antibacterial agents with multiple functional components for efficient anti-infective therapy. *Adv. Funct. Mater.* **28**, 1706709 (2018).
50. Y. Duan, H. Zheng, Z. Li, Y. Yao, J. Ding, X. Wang, J. R. Nakkala, D. Zhang, Z. Wang, X. Zuo, X. Zheng, J. Ling, C. Gao, Unsaturated polyurethane films grafted with enantiomeric polylysine promotes macrophage polarization to a M2 phenotype through PI3K/Akt1/mTOR axis. *Biomaterials* **246**, 120012 (2020).
51. X. Li, B. Cho, R. Martin, M. Seu, C. Zhang, Z. Zhou, J. S. Choi, X. Jiang, L. Chen, G. Walia, J. Yan, M. Callanan, H. Liu, K. Colbert, J. Morrissette-McAlmon, W. Grayson, S. Reddy, J. M. Sacks, H. Q. Mao, Nanofiber-hydrogel composite-mediated angiogenesis for soft tissue reconstruction. *Sci. Transl. Med.* **11**, eaau6210 (2019).
52. S. Gordon, F. O. Martinez, Alternative activation of macrophages: Mechanism and functions. *Immunity* **32**, 593–604 (2010).
53. Y. Zhao, Z. Li, S. Song, K. Yang, H. Liu, Z. Yang, J. Wang, B. Yang, Q. Lin, Skin-inspired antibacterial conductive hydrogels for epidermal sensors and diabetic foot wound dressings. *Adv. Funct. Mater.* **29**, 1901474 (2019).
54. H. Xing, X. Wang, G. Xiao, Z. Zhao, S. Zou, M. Li, J. J. Richardson, B. L. Tardy, L. Xie, S. Komasa, J. Okazaki, Q. Jiang, G. Yang, J. Guo, Hierarchical assembly of nanostructured coating for siRNA-based dual therapy of bone regeneration and revascularization. *Biomaterials* **235**, 119784 (2020).
55. P. Wang, S. Huang, Z. Hu, W. Yang, Y. Lan, J. Zhu, A. Hancharou, R. Guo, B. Tang, In situ formed anti-inflammatory hydrogel loading plasmid DNA encoding VEGF for burn wound healing. *Acta Biomater.* **100**, 191–201 (2019).
56. L. Cheng, Z. Cai, T. Ye, X. Yu, Z. Chen, Y. Yan, J. Qi, L. Wang, Z. Liu, W. Cui, L. Deng, Injectable polypeptide-protein hydrogels for promoting infected wound healing. *Adv. Funct. Mater.* **30**, 2001196 (2020).
57. H. Zhang, G. Chen, Y. Yu, J. Guo, Q. Tan, Y. Zhao, Microfluidic printing of slippery textiles for medical drainage around wounds. *Adv. Sci.* **7**, 2000789 (2020).
58. G. Chen, Y. Yu, X. Wu, G. Wang, G. Gu, F. Wang, J. Ren, H. Zhang, Y. Zhao, Microfluidic electrospray niacin metal-organic frameworks encapsulated microcapsules for wound healing. *Research* **2019**, 1–11 (2019).

Acknowledgments

Funding: This work was supported by the National Natural Science Foundation of China (81970444), Natural Science Fund for Distinguished Young Scholars of Tianjin (21JCJQJC00020), CAMS Innovation Fund for Medical Sciences (nos. 2021-I2M-1-052, 2021-I2M-1-065, and 2021-I2M-1-058), Non-profit Central Research Institute Fund of Chinese Academy of Medical Sciences (no. 2019-F40-SYS), Young Elite Scientists Sponsorship Program by Tianjin (no. TJSQNTJ-2018-01), and Tianjin Innovation and Promotion Plan Key Innovation Team of Implantable and Interventional Biomedical Materials. **Author contributions:** Conceptualization: W.L., D.K., and W.W. Methodology: Z.F., C.Z., and W.W. Investigation: W.L., R.G., W.O.-Y., and C.Y. Visualization: W.L., R.G., and X.P. Supervision: W.O.-Y., X.P., and W.W. Writing (original draft): W.L. and W.W. Writing (review and editing): W.L., P.H., C.Z, D.K., and W.W. **Competing interests:** The authors declare that they have no competing interest. **Data and materials availability:** All data needed to evaluate the conclusions in the paper are present in the paper and/or the Supplementary Materials.

Submitted 14 December 2021
Accepted 25 May 2022
Published 8 July 2022
10.1126/sciadv.abn7006